HHS Public Access

Author manuscript

J Mol Cell Cardiol. Author manuscript; available in PMC 2024 April 01.

Published in final edited form as:

J Mol Cell Cardiol. ; 177: 38–49. doi:10.1016/j.yjmcc.2023.02.005.

Caveolin-3 and Caveolae Regulate Ventricular Repolarization

Yogananda S. Markandeya[a,*], **Zachery R. Gregorich**[a,*], **Li Feng**[b], **Vignesh Ramchandran**[c], **Thomas O' Hara**[c], **Ravi Vaidyanathan**[a], **Catherine Mansfield**[d], **Alexis M. Keefe**[a], **Carl J. Beglinger**[a], **Jabe M. Best**[a], **Matthew M. Kalscheur**[a], **Martin R. Lea**[a], **Timothy A. Hacker**[a], **Julia Gorelik**[d], **Natalia A. Trayanova**[c], **Lee L. Eckhardt**[a], **Jonathan C. Makielski**[a], **Ravi C. Balijepalli**[a], **Timothy J. Kamp**[a,#]

[a)]Cellular and Molecular Arrhythmia Research Program, Department of Medicine, University of Wisconsin Madison, WI, USA

[b)]Department of Cardiology, Beijing Anzhen Hospital, Captial Medical University, National Clinical Research Center for Cardiovascular Diseases, Beijing, China

[c)]Department of Biomedical Engineering, Johns Hopkins University, Baltimore, MD, USA

[d)]National Heart and Lung Institute, Imperial College London, ICTEM, Hammersmith Hospital, Du Cane Road, London W12 0NN, UK

Abstract

Rationale: Flask-shaped invaginations of the cardiomyocyte sarcolemma called caveolae require the structural protein caveolin-3 (Cav-3) and host a variety of ion channels, transporters, and signaling molecules. Reduced Cav-3 expression has been reported in models of heart failure, and variants in *CAV3* have been associated with the inherited long-QT arrhythmia syndrome. Yet, it remains unclear whether alterations in Cav-3 levels alone are sufficient to drive aberrant repolarization and increased arrhythmia risk.

Objective: To determine the impact of cardiac-specific Cav-3 ablation on the electrophysiological properties of the adult mouse heart.

Methods and Results: Cardiac-specific, inducible *Cav3* homozygous knockout (Cav-3KO) mice demonstrated a marked reduction in Cav-3 expression by Western blot and loss of caveolae by electron microscopy. However, there was no change in macroscopic cardiac structure or contractile function. The QT_c interval was increased in Cav-3KO mice, and there was an increased propensity for ventricular arrhythmias. Ventricular myocytes isolated from Cav-3KO mice exhibited a prolonged action potential duration (APD) that was due to reductions in outward

[#] Address for correspondence: Timothy J. Kamp MD, PhD, Cellular and Molecular Arrhythmia Research Program, UW-Madison School of Medicine and Public Health, 8459 WIMR II, 1111 Highland Ave., Madison, WI 53705, (608) 263-1172 Phone, (608) 263-0405 Fax, tjk@medicine.wisc.edu.

[*]These authors contributed equally.

Disclosures

TJK is a consultant for Fujifilm Cellular Dynamics Incorporated.

potassium currents (I_{to}, I_{ss}) and changes in inward currents including slowed inactivation of $I_{Ca,L}$ and increased $I_{Na,L}$. Mathematical modeling demonstrated that the changes in the studied ionic currents were adequate to explain the prolongation of the mouse ventricular action potential. Results from human iPSC-derived cardiomyocytes showed that shRNA knockdown of Cav-3 similarly prolonged APD.

Conclusion: We demonstrate that Cav-3 and caveolae regulate cardiac repolarization and arrhythmia risk via the integrated modulation of multiple ionic currents.

Graphical Abstract

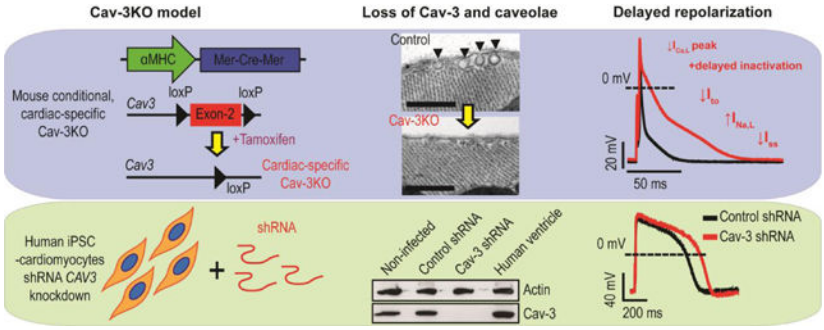

Keywords

Caveolae; Arrhythmia; Ion Channels; Cardiac Repolarization; Action Potential; Electrophysiology; Basic Science Research; Animal Models of Human Disease

1. Introduction

Caveolae are 50–100 nm flask-shaped invaginations in the plasma membrane that have been implicated in a variety of essential cellular processes, including endocytosis, mechanotransduction, excitability, and signaling [1–3]. Caveolin-1 (Cav-1) and Caveolin-3 (Cav-3) are structural proteins that stabilize caveolar structures along with more recently identified Cavins [2]. Cav-3 is expressed primarily in muscle cells, including cardiac, skeletal and smooth muscle; whereas, expression of Cav-1 is more broadly distributed. It is debated whether Cav-1 is expressed in cardiomyocytes [4, 5], but recent evidence suggests that Cav-1 is present in cardiomyocytes and generates a distinct population of caveolae in the T-tubules and at the intercalated discs [6]. How these distinct pools of caveolae regulate cardiac biology and disease remains incompletely understood.

A range of different ion channels have been proposed to interact with Cav-3, including L-type Ca^{2+} channels ($Ca_v1.2$), T-type Ca^{2+} channels ($Ca_v3.2$), Na^+ channels ($Na_v1.5$), pacemaker channels (HCN4), and several K^+ channels (e.g., $K_v1.5$, $K_v7.1$, $K_{ir}6.2$, and $K_{ir}2.1$) [7–9]. A reduction in Cav-3 expression has been observed in several experimental models of heart failure. For example, a combined pressure and volume overload rabbit model of heart failure results in an 80% decrease in Cav-3 protein levels along with QT interval prolongation and increased ventricular arrhythmias [10–12]. Transgenic overexpression of Cav-3 was shown to mitigate heart rate-corrected QT (QT_c) interval prolongation following adrenergic challenge in mice with cirrhotic cardiomyopathy [13]. In

addition, several variants in the human gene encoding Cav-3, *CAV3,* have been putatively associated with the congenital long QT syndrome, and these LQTS-associated *CAV3* variants produce changes in multiple ionic currents that, in combination, prolong the ventricular action potential duration (APD) and hence QT_c [14–16]. These findings raise the question of whether alterations in Cav-3 levels alone are sufficient to drive the changes in ventricular repolarization observed in certain forms of heart disease and impact the arrhythmia risk.

To probe the functional role of Cav-3, prior studies have described embryonic *Cav3* knockout mice which are viable, fertile, and develop a mild but progressive cardiomyopathy marked by cardiac hypertrophy, dilation, and reduced fractional shortening [5, 17]. Nevertheless, the use of traditional constitutive *Cav3* knockouts in these studies complicates the interpretation of the cardiac effects of Cav-3 loss because of the impact of confounding factors, such as compensatory changes during development or the secondary impact from Cav-3 loss in other tissues, including skeletal and smooth muscle. Previously, we described the first cardiomyocyte-specific, conditional *Cav3* knockout mouse, which overcomes some of these limitations; however, analysis was restricted to isolated ventricular cardiomyocytes and the regulation of L-type Ca^{2+} channels [18].

In this study, we examine the impact of cardiac-specific loss of Cav-3 expression in the adult mouse heart on cardiac structure, function, and electrophysiology. We show that the cardiac-specific Cav-3 knockout (Cav-3KO) mice do not develop structural remodeling or left ventricular dysfunction in contrast to embryonic Cav-3 knockout models, but the mice do exhibit a prolonged QT_c and an increased susceptibility to ventricular arrhythmias. We observe an increase in the APD in isolated ventricular myocytes due to significant changes in both inward and outward currents. We further demonstrate that APD is prolonged in human induced pluripotent stem cell-derived cardiomyocytes (hiPSC-CMs) upon shRNA-mediated Cav-3 knockdown, which suggests that Cav-3 modulates cardiac repolarization in human myocytes as well. Collectively, our results show that Cav-3 and caveolae are critical regulators of ventricular repolarization and thus arrhythmia risk.

2. Materials and methods

2.1. Animals

All procedures involving animal care and handling were reviewed and approved by the University of Wisconsin School of Medicine and Public Health Animal Care and Use Committee. Animals were handled in accordance with the NIH Guide for the Care and Use of Laboratory Animals. Transgenic animals were generated at the University of Wisconsin Biotechnology Center Transgenic Animal Facility. Cardiac-restricted conditional *Cav3* knockout mice were generated by targeting Exon 2 of the *Cav3* gene, using homologous recombination in murine SV/129 R1 embryonic stem cells to introduce a cassette containing loxP sites flanking Exon 2 with a neomycin selection cassette. Positive recombinants were microinjected into C57BL/6 blastocysts to produce chimeric founders. Chimeric founders were mated to C57BL/6J females, F1 pups were PCR genotyped, and the mice were backcrossed on a 129S2 (Charles Rivers) background for at least 10 generations. The cardiac-specific αMHC-MerCreMer mice [19] maintained in the C57/Bl6 background for

at least 10 generations were crossed with heterozygous floxed *Cav3* mice (*Cav3*$^{fl/WT}$)to produce *Cav3*$^{fl/WT; MerCreMer}$ mice that were then bred to produce *Cav3*$^{fl/fl;MerCreMer}$, *Cav3*$^{fl/WT;MerCreMer}$, and *Cav3*$^{WT/WT;MerCreMer}$ mice. These mice were fed Tamoxifen (Tam) chow (0.5 mg Tam per gram of chow) for 7 days followed by normal chow to generate cardiac-specific Cav-3KO, Cav-3Het, and control mice, respectively.

2.2. Western blot

Whole-cell lysates were prepared from left ventricular tissue, proteins were separated by SDS-PAGE (4–15% gradient gels; Bio-Rad, USA), and transferred to PVDF membranes. Membranes were blocked in tris-buffered saline with 0.1% tween 20 (TBST) containing 5% nonfat milk followed by incubation overnight at 4 °C with primary antibodies (anti-Cav-3 and -K_{ir}2.1 were from BD Biosciences, USA; anti-GAPDH was from EMD Millipore, USA; anti-Ca_v1.2 was from Alomone Labs, Israel; and anti-K_v4.2, -K_v4.3, -K_v1.5, and -K_v2.1 were from NeuroMab, USA). Blots were then incubated with horseradish peroxidase-conjugated secondary antibodies (GE Healthcare, USA) and visualized with enhanced chemiluminescence regent (GE Healthcare).

Preparations of crude membrane extracts—Hearts were excised from anesthetized Tam-fed WT and Cav-3KO mice, the atria were removed, hearts were opened, quickly rinsed in PBS to remove blood, and immediately snap frozen in liquid nitrogen. Frozen heart tissue was ground to powder under liquid nitrogen using a pre-cooled mortar and pestle and immediately transferred to 50 mL conical centrifuge tubes containing ice-cold homogenization buffer [4 mM HEPES pH 7.5, 320 mM sucrose, 1 mM EDTA pH 8, 1X cOmplete, mini, EDTA-free protease inhibitor cocktail (cat# 11836170001; Sigma-Aldrich, St. Louis, MO, USA), and 1 mM PMSF. Subsequently, tissue was further broken up by 5 × 15 sec bursts with a Polytron PT 1200 E Handheld homogenizer (Kinematica, Bohemia, NY, USA). An aliquot of the resulting lysate was removed and saved as the “total protein” fraction. Tissue lysates were centrifuged 1000 × g for 10 min at 4 °C to pellet nuclei and large tissue/cell debris. The supernatants were transferred to Open-Top Thinwall Ultra-Clear Tubes (cat# 344059; Beckman Coulter, Brea, CA, USA), diluted to a final volume of 12 mL by adding ice- cold PBS with 1X cOmplete, mini, EDTA-free protease inhibitor cocktail (cat# 11836170001; Sigma-Aldrich), and centrifuged 106,882.9 × g for 75 min at 4 °C to pellet the membranes. An aliquot of the supernatant was removed and saved as the “cytosolic protein” fraction and the remaining supernatant was discarded. The pellet, which contains the cardiac membranes, was resuspended in RIPA buffer [50 mM Tris-HCl pH 8, 150 mM NaCl, 1 mM EDTA pH 8, 1% triton X-100, 0.5% SDS, 0.75% sodium deoxycholate, 1X cOmplete, mini, EDTA-free protease inhibitor cocktail (Sigma-Aldrich), and 1 mM PMSF] by pipetting up and down several times, mixing by end-over-end rotation for 30 min at 4°C, and finally sonicating using a Fisherbrand Model 120 Sonic Dismembrator (Thermo Fisher Scientific, Waltham, MA, USA) with 3 × 10 sec bursts at 30% amplitude. The resulting lysate was saved as the “membrane fraction.” The protein content of the total, cytosolic, and membrane fractions was determined prior to SDS-PAGE using Bio-Rad Protein Assay Dye Reagent Concentrate (cat# 5000006) in accordance with the manufacturer’s instructions. For Western blot analysis, 20–25 μg of protein fractions were resolved by SDS-PAGE and transferred to Amersham Hybond P Western blotting

membrane (0.45 um pore size, cat# GE10600023; MilliporeSigma, Burlington, MA, USA) at 10 V overnight in a cold room (4 °C). After transfer, total protein loading was assessed by staining with Revert 700 Total Protein Stain (cat# 926–11010, LI-COR, Lincoln, NE, USA) in adherence with the manufacturer's instructions. Western blotting was carried out as described above.

2.3. Histology

Hearts were excised from anesthetized mice, washed with PBS to remove excess blood, and fixed in phosphate buffer (pH = 7.4) with 4% paraformaldehyde for 24 hr. Fixed heart tissue was dehydrated by treatment with 70% ethanol for 24 hr and embedded in paraffin wax using standard procedures. Tissue sections were stained with hematoxylin & eosin or Masson's trichrome stain to assess fibrosis.

2.4. Electron microscopy

Hearts were excised from anesthetized mice, perfused with PBS to remove excess of blood, and then perfused with fixative solution (PBS with 4% paraformaldehyde and 0.1% glutaraldehyde). Ultrathin (~60 nm) sections were post-fixed with OsO_4, and stained with uranyl acetate and lead citrate. Samples were examined under a PHILIPS CM120 transmission electron microscope as previously described [20].

2.5. Echocardiography

Echocardiography was performed in a subset of Cav-3KO, Cav-3Het, and control mice before and after Tam treatment. Transthoracic echocardiography was performed using a Visual Sonics Vevo 770 Micro-ultrasound imaging system with a 30 MHz transducer as detailed previously [21]. Mice were sedated by facemask administration 1% isoflurane and maintained on a heated platform in a left lateral decubitus position. End diastolic and systolic left ventricular diameters, as well as anterior and posterior wall thicknesses, were measured on line from M-mode images using the leading edge-to-leading edge convention. Echocardiography data were analyzed blinded to genotype of the animal.

2.6. Telemetry ECG recording

ECG telemetry transmitters ETA-F10 (Data Science International, USA) were surgically implanted in Cav-3KO, Cav-3Het, and control mice. One week after surgery, a receiver was placed under the cage of each animal and ECG signals were recorded in freely moving mice continuously for 24 hr. Signals were then analyzed using commercially available software from NOTOCORD, France). The mice were then treated with Tam for one week. Following a two week recovery period, ECGs were again recorded for an additional 24 hr interval. Heart rate, PR interval, and QT intervals were measured manually for the one hr time period between 9–10 am. Telemetry data were analyzed blinded to genotype. Reported QT intervals were corrected for heart rate as previously published for conscious mice [22].

2.7. Programmed electrical stimulation

In vivo electrophysiological measurements were carried out in mice to assess arrhythmia susceptibility. Mice were anesthetized by facemask administration of 2% isoflurane,

maintained on a heated platform, and surface ECGs were recorded from 27-gauge needle electrodes that were inserted subcutaneously in the standard limb lead positions. The heart rate and rhythm were recorded continuously throughout the procedure. Ventricular burst stimulation generated by a Grass stimulator (Model S48; Natus Neurology Incorporated, USA) was administered via platinum electrodes placed at the apex of the heart and the right ventricular outflow tract. Arrhythmias were generated using a burst pacing stimulus using a voltage just greater than the capture threshold for 2 ms pulses at a frequency between 1000–1500 pulses per sec for trains lasting 2 sec given at 10 sec intervals [23].

2.8. Cardiomyocyte isolation

Single ventricular myocytes were isolated by enzymatic digestion as previously described [9]. Briefly, hearts were excised from anesthetized male mice, the aorta was cannulated, and hearts were perfused using a Langendorff perfusion system. Initially, heart were perfused with zero Ca^{2+} Tyrode's solution containing (mmol/L): 137 NaCl, 5 KCl, 1 $MgCl_2$, 10 glucose, and 10 HEPES, pH 7.4 for 5 min, followed by Tyrode's solution containing 1 mg/ml collagenase type-II (Worthington Biochemical Corporation, USA) for 10–12 min at 37 °C. Left ventricle tissue was dissected out, several pieces of myocardium were selected and placed in petri dishes with Tyrode's solution containing 10% FBS. Single myocytes were released by gentle trituration and collected in Tyrode's solution with 5% FBS. Ca^{2+} was reintroduced in a step-by-step manner up to a 1 mM final concentration.

2.9. Cellular electrophysiology

Myocytes were placed in an RC-22 perfusion chamber (Warner Instruments, USA) mounted on an inverted NikonTE200 microscope (Nikon, USA). Single healthy rod-shaped cardiomyocytes were randomly selected for electrophysiological measurements. Cardiomyocyte capacitance, action potentials, and ionic currents were measured via the whole-cell patch clamp method using an Axopatch200B amplifier (Axon Instruments, USA) connected with A/D converter Digidata 14440A (Axon Instruments). Data were acquired from ClampX10.3 (Molecular Devices, USA) and analyzed with Clampfit10.3 (Molecular Devices). Patch pipets (1.5–2.5 MΩ resistance) were pulled from thin-walled borosilicate glass capillaries (World Precision Instruments, USA) with a programmed P-97 shutter puller (Sutter Instrument Company, USA). The data were filtered at 5 kHz and digitized at 50 kHz. The current traces were corrected for linear capacitance and leak using P/4 subtraction unless otherwise mentioned. Voltage clamp experiments were carried out at room temperature and current clamp experiments were performed at 35 ± 2 °C. External and internal pipette buffers are listed in Table S1 and Table S2, respectively. Membrane potential was corrected for the liquid junction potential, which was calculated using Clampex 10.1 (Axon Instruments). The calculated junction potential was 5 mV for mouse ventricular myocyte and 4 mV for iPSC-CM current clamp experiments. These experiments were not blinded to genotype given the need to identify animals or cells for study.

2.10. Optical mapping of mouse hearts

The mouse heart was rapidly explanted and rinsed free of blood in ice-cold oxygenated Krebs-Henseleit (KH) solution (128.2 mM NaCl, 4.7 mM KCl, 1.05 mM $MgCl_2$, 1.3 mM $CaCl_2$, 1.19 mM KH_2PO_4, 20 mM $NaHCO_3$, and 11.1 mM glucose and equilibrated

with 95% O_2 + 5% CO_2) containing heparin (12 U/ml). The heart was transferred to a Langendorff system, where the aorta was cannulated and the heart perfused with oxygenated KH solution. A small silicon tube was inserted into the left ventricle through the pulmonary veins. The heart was perfused at a fixed flow rate (~5 ml/min) at 37 °C. Following a 15-minute stabilization period, the heart was stained with the voltage-sensitive dye RH237 (1 mg/ml in dimethyl sulfoxide (DMSO)), the calcium-sensitive dye Rhod-2AM (1 mg/ml in DMSO mixed 1:1 with 20% Pluronic), and perfused with the excitation-contraction uncoupler blebbistatin (10 μM) to eliminate motion artifact. The heart was excited using 530-nm light-emitting diodes, and emitted light was collected using a CMOS camera. Signals were recorded from the left ventricular free wall during pacing at 400 beats per minute (1 mA). Optical mapping data was analyzed using a custom written MATLAB script as described previously [24, 25].

2.11. iPSC-derived cardiomyocytes and shRNA knockdown

iCell cardiomyocytes were obtained from Cellular Dynamics International's (CDI) Madison, USA. The vial containing iCell cardiomyocytes were thawed at 37 °C in a water bath for 1 min and transferred to 50 mL falcon tube containing iCell Cardiomyocytes Plating Medium (iCPM, CDI) as described in the manufacturer protocol. The iCell cardiomyocytes were plated on 0.1% gelatin-coated coverslips or 6-well plates. After 48 hr, the culture medium was replaced with iCell Cardiomyocyte Maintenance Medium (iCMM, CDI). iCMM was replaced every other day. For Western blot experiments 5×10^5 cells were plated in one well of a 6-well plate. For electrophysiology experiments, cells were plated on 0.1% gelatin-coated coverslips. Cav-3 knockdown, was performed by transducing iCell using shRNA Cav-3 lentiviral particle pLKO.1-CMV-tGFP (sigma Aldrich USA) along with scrambled shRNA Control Lenti viral particles. All the experiments were carried out after 72 hr of viral transduction. Electrophysiology experiments were carried out in cells expressing eGFP. Immunostaining was performed using specific antibodies: anti-Cav-3 mouse (Abcam ab2912 USA), Anti-Actin (α-Sarcomeric) (A-2172, Sigma), DAPI sigma 33342, Rabbit Cav-3 (abcam, USA), secondary antibodies Alexa-647 & Alexa-568 (Invitrogen, Thermo Fisher Scientific, USA). Confocal imaging was performed using a Leica SP-8 confocal microscope.

2.12. Mathematical modeling

Electrophysiological simulations used the Morotti et al. 2014 mouse ventricular myocyte model [26]. Numerical calculations were executed with Matlab code that Stefano Morotti generously shared with us, modified from baseline (WT) to represent Cav-3KO as follows. For ion channel currents that were affected by Cav-3KO in our experiments, model conductance was adjusted based on summary data of the Cav-3KO/WT peak current ratio (Fig. 5A): late Na^+ current ($I_{Na,L}$, Cav-3KO conductance was 10-fold that of WT), L-type Ca^{2+} current ($I_{Ca,L}$, Cav-3KO conductance was 21% of WT), transient outward K^+ current (I_{to}, 43% of WT), steady state outward K^+ current (I_{ss}, 57% of WT), slowly inactivating K^+ current ($I_{K,slow}$, 81% of WT). Additionally, experiments demonstrated gating changes in $I_{Ca,L}$, observed as shifts in $V_{-1/2}$ for steady state activation and inactivation curves. These shifts relative to WT were included in the Cav-3KO model (activation: V-dependence of dss was shifted right by 4.9655 mV, inactivation: V-dependence of fss was shifted left by 4.6996

mV). With this Cav-3KO representation, the time dependence of relative $I_{Ca,L}$ current was accurately reproduced (Fig. 5B).

2.13. Statistics

Data are presented as mean ± S.E.M. All data were analyzed using statistical software Origin 9.0.0 (Origin Lab Corporation, USA). Statistical significance was determined by student *t*-test for accessing the difference between two groups and one-way ANOVA for multiple groups with post hoc testing using Tukey method. $P < 0.05$ was considered statistically significant.

3. Results

3.1. Cardiac-specific Cav3 ablation decreases Cav-3 expression and caveolae abundance

To investigate the role of Cav-3 in the heart, as well as avoid the drawbacks associated with embryonic constitutive knockout models, we generated cardiac-specific, inducible *Cav3* knockout mice. Mice with the αMHC-MerCreMer transgene were crossed with mice containing loxP sites flanking Exon 2 of *Cav3*. Male 8–10 week old double transgenic mice were fed a diet with Tam for 1 week followed by 2 weeks of normal chow (Fig. 1A), to disrupt one allele or both alleles of *Cav3* in cardiomyocytes, referred to as Cav-3Het or Cav-3KO, respectively. Control (Con) mice were produced by the same Tam administration protocol to αMHC-MerCreMer mice with wild-type *Cav3*. Knockout of *Cav3* was evaluated at the protein level by Western blot analysis, which showed a significant reduction in Cav-3 expression levels in Cav-3KO (62%), compared to Con mice, and an intermediate level in Cav-3Het (Fig. 1B). The residual Cav-3 expression in the Cav-3KO reflects expression of Cav-3 in noncardiomyocytes such as vascular smooth muscle cells, although we cannot exclude a small fraction of cardiomyocytes continue to express Cav-3. The more variable results in the Cav-3Het did not lead to a significant reduction in Cav-3 and may reflect variable degrees of compensation by the wild-type allele. Furthermore, the induced deletion of *Cav3* Exon 2 did not result in any detectable expression of truncated mutant Cav-3 protein (Fig. S1). Since Cav-3 is essential for the formation of caveolae in cardiac muscle [5, 27], transmission electron microscopy (TEM) was employed to examine caveolae in cardiac muscle from Cav-3KO, Cav-3Het, and Con mice (Fig. 1C). A significant decrease in the number of morphologically identifiable caveolae in the surface sarcolemma of Cav-3KO (~15% of Con) and Cav-3Het (~43% of Con), was observed (Fig. 1D). Echocardiography was performed to determine if Cav-3 ablation impacted cardiac structure or function in adult mice. Eight weeks after Tam treatment, Cav-3KO mice showed no significant differences in LV mass, fractional shortening (FS), ejection fraction (EF), left ventricular internal dimension at end-diastole (LVIDd), or thickness of diastolic left ventricular posterior wall (LVPWd) compared to Con (Fig. 1E). Heart weight-to-body weight (HW/BW) ratios did not differ between Cav-3KO and Con mice (Fig. 1F). Histology revealed no difference in cardiac structure or fibrosis in sections from the hearts of Cav-3KO and Con mice (Fig. 1G). Collectively, these results demonstrate that cardiac-specific ablation of *Cav3* in adult mice leads to loss of Cav-3 protein expression and morphologically identifiable caveolae without affecting macroscopic cardiac structure or contractile function.

3.2. Cav3 ablation prolongs QTc interval and increases susceptibility to ventricular arrhythmia

Given that Cav-3 expression is reduced in some models of heart failure that are associated with QT prolongation, as well as the fact that *CAV3* variants have been identified in patients with inherited long QT syndrome [12, 14, 28–31], we next assessed the impact of *Cav3* ablation on the electrical activity of the heart. *In vivo* telemetric ECG was recorded in conscious Con and Cav-3KO mice for before and after Tam treatment. The QTc was significantly prolonged in Cav-3KO mice following Tam treatment but the QTc was unchanged in Tam-treated Con mice (Fig. 2A and B). Cav-3KO mice displayed no difference in average spontaneous heart rate_or PR interval relative to Con mice (Fig. 2A and B). To determine whether loss of Cav-3 also increases the propensity for arrhythmia, Con and Cav-3KO mice were subjected to burst pacing and monitored by ECG. The occurrence of ventricular tachycardia (VT) was significantly increased in Cav-3KO (8/9) mice compared to Con (0/5) (Fig. 2C and D). These results demonstrate that loss of Cav-3 expression and caveolae in the heart prolongs ventricular repolarization and increases susceptibility to VT.

3.3. Prolonged APD in isolated Cav-3KO myocytes, contribution of repolarizing K^+ currents

To assess the impact of Cav-3 loss on APD, whole-cell patch clamp experiments were performed on freshly isolated adult ventricular myocytes from Cav-3KO, Cav-3Het, and Con mice. In Cav-3KO myocytes, APD at 50% (APD50) and 90% (APD) repolarization were significantly prolonged compared to Con (Fig. 3A, Table S3). The APD50 and APD90 from Cav-3Het mice on average trended longer than Con, but the differences were not statistically significant (Fig. 3B, Table S3). The resting membrane potential (RMP) did not differ between the three groups (Fig. 3B, Table S3). The RMP values ranging from −63 to −70 mV for all groups were more depolarized than those observed under more physiological recording conditions without intracellular dialysis, but the stable recordings on quiescent cells showed reproducible data. To confirm that APD prolongation was present in the native heart, we used high-resolution optical mapping of membrane voltage and intracellular Ca^{2+} in Langendorff-perfused whole mouse hearts and found significant prolongation of APD50 and APD70, but not APD90, in Cav-3KO mice in agreement with the single cell data (Fig. S2). Conduction velocity and intracellular Ca^{2+} transients were similar between Con and Cav-3KO mice (Fig. S2).

In the heart, APD is controlled by a delicate balance between repolarizing and depolarizing currents; and disruption of this balance can lead to prolongation of the APD and arrhythmia. Therefore, we hypothesized that Cav-3 loss reduces repolarizing voltage-gated K^+ (K_v) currents, leading to APD prolongation. To test this hypothesis, we first measured total outward K_v current (I_K) in Cav-3KO and Con myocytes using whole-cell voltage clamp. In Cav-3KO myocytes, we observed a significant decrease in I_K relative to Con (Fig. 3C). The current-voltage (I-V) relationships revealed a significant reduction in I_K density across the full range of test potentials in Cav-3KO myocytes compared to Con (Fig. 3C).

Prior studies have shown that, in adult mouse ventricular myocytes, I_K consists of up to four distinct K_v currents, namely the transient outward K^+ current with fast inactivation ($I_{to,f}$), transient outward K^+ current with slow inactivation ($I_{to,s}$), slowly inactivating K^+ current ($I_{K,slow}$), and the non-inactivating steady-state K^+ current (I_{ss}) [32]. To estimate the relative contributions of $I_{to,f}$, $I_{K,slow}$, and I_{ss} to I_K in Cav-3KO and Con myocytes, we employed the method described by Xu et al. [32]. The mean $I_{to,f}$ current density at +40 mV test potential was significantly decreased in Cav-3KO (11.3 ± 2.0 pA/pF) compared to Con (24.1 ± 3.4 pA/pF) (Fig. 3D). Likewise, mean I_{ss} current density was also decreased in Cav-3KO (3.4 ± 0.6 pA/pF) with respect to Con (6.1 ± 0.4 pA/pF); however $I_{K,slow}$ (7.1 ± 1.0 pA/pF and 8.0 ± 1.1 pA/pF in Cav-3KO and Con, respectively) did not differ between groups (Fig. 3D).

The inward rectifying K^+ current (I_{K1}) maintains the resting membrane potential and contributes to phase 3 repolarization [33–35]. Therefore, we determined whether *Cav3* ablation impacts I_{K1} currents in Cav-3KO ventricular myocytes. In our experiments, I_{K1} currents in Cav-3KO myocytes were not different than in Con (Fig. 3E). The I-V relationships for I_{K1} current density established in Cav-3KO and Con myocytes were superimposable, which was in agreement with the observation that RMP did not differ in these cells (Fig. 3B).

We hypothesized that decreased K^+ current density in Cav-3KO myocytes was a consequence of decreased K^+ channel expression. However, Western blot analysis revealed that the normalized protein levels of relevant K^+ channels were not different in Cav-3KO and Con mouse whole myocardium lysates (Fig. 3F). In addition, we evaluated for expression of the K_v4 channel subunit, KChIP2, in whole heart lysates and membrane lysates and found no difference between Cav-3KO and Con (Fig. S3). Collectively, these results suggest that Cav-3 loss, in part, prolongs APD by reducing $I_{to,f}$ and I_{ss} independent of changes in K^+ channel protein expression.

3.4. Alterations in inward currents contribute to APD prolongation in isolated Cav-3KO myocytes

In addition to decreases in repolarizing K^+ currents, increases in depolarizing $I_{Na,L}$ or $I_{Ca,L}$ currents, which flow after the upstroke of the action potential can contribute to APD prolongation. We have previously shown that LQTS9-causing mutations in Cav-3 augment $I_{Na,L}$ and differentially modulate $I_{Ca,L}$ [14, 36]; thus, we next sought to determine whether $I_{Na,L}$ or $I_{Ca,L}$ are altered in left ventricular myocytes from Cav-3KO mice using whole-cell patch clamp.

Peak I_{Na} did not differ significantly in Cav-3KO and Con myocytes. The I_{Na}-V relationships established in these cells were superimposable at all test potentials despite some lack of voltage control given the large current magnitudes (Fig. 4A). While peak I_{Na} underlies excitability, there is a residual I_{Na}, referred to as $I_{Na,L}$, flowing after the peak that, together with $I_{Ca,L}$, maintains depolarization during phase 2 of the cardiac action potential. Prior studies have shown that Sudden Infant Death Syndrome (SIDS)- and LQT-causing variants in *CAV3* potentiate $I_{Na,L}$ [14, 30]. Thus, it is conceivable that increased $I_{Na,L}$ could contribute to APD prolongation in Cav-3KO myocytes. To determine whether $I_{Na,L}$ is

affected by loss of Cav-3, we measured TTX-sensitive $I_{Na,L}$ in Cav-3KO and Con myocytes. We found that, $I_{Na,L}$ was increased by 5-fold in Cav-3KO myocytes at a test potential of −20 mV (100.6 ± 15 A*ms*F^{-1}) compared to Con (19.66 ± 10 A*ms*F^{-1}) (Fig. 4B). Consistent with the lack of change in peak I_{Na}, we did not observe a change in the expression of $Na_v1.5$ at the protein level by Western blot (Fig. 4F).

On the other hand, $I_{Ca,L}$ was significantly decreased in Cav-3KO myocytes in comparison to Con (Fig. 4C). I-V relationships indicated that peak $I_{Ca,L}$ (at a test potential of 0 mV) was reduced by 28% in Cav-3KO (−6.5 ± 0.3 pA/pF) compared to Con (−9.1 ± 0.5 pA/pF) myocytes. The voltage dependence of channel activation exhibited a small but significant depolarizing shift in the Cav3-KO cells (Fig. 4D). However, $I_{Ca,L}$ inactivation was slower in Cav-3KO compared to Con myocytes (Fig. 4D). As an independent quantitative measure of $I_{Ca,L}$ inactivation, we determined the ratios of current remaining at 50 ms (r50), 100 ms (r100), and 200 ms (r200) relative to the peak current. The r50, r100, and r200 measures were significantly increased in Cav-3KO myocytes confirming a slowing of inactivation (Fig. 4D). The steady-state inactivation of $I_{Ca,L}$ measured after a 500 ms prepulse was shifted slightly to more negative potentials in Cav-3KO myocytes (Fig. 4E). These changes in $I_{Ca,L}$ demonstrate a change in gating of the $Ca_v1.2$ channels in response to *Cav3* ablation. Moreover, we did not detect any difference in $Ca_v1.2$ protein expression by Western blot between Cav-3KO and Con from whole heart lysates (Fig. 4F) or membrane-enriched preparations (Fig. S3C).

3.5. Numerical simulation

To investigate if the observed changes in measured ionic currents in Cav-3KO myocytes adequately account for the changes in APD, we developed a computational representation of the Cav-3KO myocyte action potential based on the Morotti et al. mouse ventricular myocyte model [26]. Experimental data from isolated Cav-3KO and Con myocytes were incorporated into the Morotti et al. mouse ventricular cell model and individual ionic currents ($I_{Ca,L}$, $I_{K,slow}$, I_{ss}, $I_{Na,L}$, and $I_{to,f}$) were simulated as shown in Fig. 5A. Subsequently, these currents were used to simulate action potentials at a frequency of 1 Hz (Fig. 5C). Similar to the action potentials measured in isolated ventricular myocytes from Cav-3KO mice, action potentials simulated using individual ionic current data from Cav-3KO myocytes were significantly prolonged in comparison to Con (Fig. 5C). Both APD50 and APD90 were increased in simulated Cav-3KO myocytes relative to Con (Fig. 5C), which corroborates experimental results from isolated ventricular myocytes. These findings suggest that *Cav3* ablation-induced alterations in function of the characterized ionic currents that underlie the APD prolongation in Cav-3KO myocytes.

3.6. Cav-3 knockdown delays repolarization in hiPSC-CMs

Since there are known differences in the ionic currents responsible for generating the human and mouse ventricular action potentials, we next sought to determine whether loss of Cav-3 affects the human ventricular action potential in a similar manner to the mouse action potential. To test this, we took advantage of hiPSC-CMs. We have previously shown that these hiPSC-CMs have ionic currents and channel gating properties underlying their action potentials similar to those reported for human cardiomyocytes, although exhibit an immature

phenotype [37]. First, to determine whether hiPSC-CMs have morphologically identifiable caveolae and express Cav-3, TEM and Western blot analyses were carried out on day 30 (post-differentiation) cultured hiPSC-CMs. TEM analysis revealed the presence of surface membrane invaginations characteristic of caveolae (Fig. 6A, indicated by arrow heads) and Western blot analysis confirmed Cav-3 expression (Fig. 6B) in these cells. Next, to ascertain whether Cav-3 is involved in repolarization in human cardiomyocytes, action potentials were recorded in hiPSC-CMs infected with lentivirus carrying control or Cav3-targeted shRNA. The hiPSC-CMs infected with lentivirus carrying Cav-3-targeted shRNA showed near complete loss of Cav-3 protein expression on Western blot analysis (Fig. 6B) and loss of Cav-3 immunofluorescence with confocal imaging (Fig. S4). Both APD50 and APD90 were significantly prolonged in hiPSC-CMs with shRNA-mediated Cav-3 knockdown compared to Con with no difference in MDP in these cells (Fig. 6C and D). Together these results suggest that hiPSC-CMs express Cav-3, have morphologically identifiable caveolae, and exhibit action potential prolongation upon Cav-3 knockdown.

4. Discussion

In this study, we evaluated the impact of cardiac-specific knockout of *Cav3* on the electrophysiological properties of the adult mouse ventricle. Loss of Cav-3 did not impact resting ventricular function or ventricular structure, in contrast to embryonic *Cav3* knockout models [27]. However, we did observe a significant prolongation of the QT_c interval in Cav-3KO mice and increased susceptibility to ventricular arrhythmias triggered by electrical stimulation. The increased QT_c was secondary to ventricular APD prolongation due to changes in a variety of both outward and inward currents that regulate cardiac repolarization. Specifically, a remarkable decrease in repolarizing K^+ currents, I_{to} and I_{ss}, as well as an increase in $I_{Na,L}$ and delayed inactivation of $I_{Ca,L}$, slowed repolarization. These experimental observations were adequate to explain APD prolongation based on mathematical modeling of the mouse ventricular action potential. Finally, we demonstrate that loss of Cav-3 in hiPSC-CMs likewise prolongs APD extending the relevance of these findings to the human heart. Overall, these results link Cav-3 levels and hence caveolae to a program of integrated regulation of cardiac repolarization and arrhythmia risk.

4.1. Reduced I_{to} and I_{ss} in Cav-3KO cardiomyocytes

In mouse ventricular myocytes, I_{to} is the dominant repolarizing current, and Cav-3KO myocytes exhibited approximately a 40% decrease in I_{to} relative to Con. Even though I_{to} has a questionable role in regulating APD in large animal and human ventricles, one of the most common and reproducible cellular electrophysiological findings in human heart failure and large animal dilated cardiomyopathy models is a reduction in I_{to} [38, 39]. Two distinct forms of I_{to}, $I_{to,f}$ and $I_{to,s}$, have previously been defined in mouse ventricle based on the kinetics of current decay [32]. $I_{to,f}$ was characterized in our study given its broad distribution in the left ventricle, and we avoided isolation of cells from the interventricular septum, which are the only ventricular cardiomyocytes that exhibit $I_{to,s}$ [32]. $K_V4.2$ and $K_V4.3$ potassium channels generate $I_{to,f}$ in mouse hearts [40], and Alday et al. previously reported that a subpopulation of $K_V4.2/K_V4.3$ channels interact with Cav-3 and are localized to caveolae in rat ventricular myocytes [41]. The caveolar localization of $K_V4.2$ and $K_V4.3$ is essential for regulation of I_{to}

by α_1-ARs [41]. Moreover, we recently reported that the Cav-3 variants associated with QT prolongation, F97C and S141R, reduce $I_{Kv4.2}$ and $I_{Kv4.3}$ expressed in HEK293 cells, in part, as a result of significant changes in the voltage-dependent gating of these channels [36]. Thus, the findings of prior studies are consistent with Cav-3 and caveolae regulating I_{to} as observed in the Cav-3KO mouse. We did not observe measurable changes in the expression of $K_v4.2$, $K_v4.3$ or KChIP2 proteins in the Cav-3KO mouse relative to Con suggesting that changes in gating of the channels may be the predominant factor in the reduction in current levels. However, further studies will be needed to determine the specific mechanisms and potential signaling pathways involved.

In addition to I_{to}, $I_{K,slow}$ and I_{ss} contribute approximately 30% and 10%, respectively, to the peak outward K^+ current in adult mouse left ventricular apex cells [32]. Although $I_{K,slow}$ density did not differ in Cav-3KO and Con myocytes, we detected a 40% reduction in I_{ss} in Cav-3KO myocytes. $I_{K,slow}$ consists of two distinct currents, $I_{K,slow1}$ ($K_v1.5$) and $I_{K,slow2}$ ($K_v2.1$) [40]. Interestingly, studies have previously reported that $K_v1.5$ channels can interact with Cav-3 and localize to caveolae in heterologous expression systems [42, 43]. However, in native cardiac tissue from rat and dog, Eldstrom et al. failed to detect an interaction between $K_v1.5$ and Cav-3 [44], suggesting that these channels do not localize to caveolae in cardiomyocytes. Similarly, there is general agreement that $K_v2.1$ channels localize to non-caveolar lipid rafts [45]. Given that $K_v1.5$ and $K_v2.1$ channels do not appear to localize to caveolae, it is perhaps not surprising that $I_{K,slow}$ was unaltered in Cav-3KO myocytes. There remains no clear consensus on the identity of the channel(s) responsible for I_{ss}, so future studies will be needed to define the molecular mechanisms of Cav-3 regulation of this current.

I_{K1} sets the resting membrane potential and contributes to phase 3 repolarization of the ventricular action potential. Pathogenic variants in this channel can prolong APD [46]. We did not find any difference in I_{K1} current density between Cav-3KO and Con myocytes, which is in agreement with the fact that resting membrane potential did not differ in these cells. These results demonstrate that changes in I_{K1} are not responsible for action potential prolongation in Cav-3KO myocytes—a finding that is consistent with the results of a previous heterologous expression study demonstrating that co-expression of WT Cav-3 with $K_{ir}2.1$ does not affect I_{K1} density [47]. Nevertheless, these previous studies did suggest that Cav-3 can interact and co-localize with $K_{ir}2.1$ and $K_{ir}2.2$ [47, 48]. Furthermore, co-expression of the Cav-3-F97C variant with $K_{ir}2.1$ or $K_{ir}2.2$ in HEK293 cells leads to decreased cell surface expression of $K_{ir}2.1$ or $K_{ir}2.2$, concomitant with reduced I_{K1} [47, 48]. Thus, although our initial assessment of the impact of Cav-3KO on I_{K1} shows no impact on current density, it does not exclude the possibility that Cav-3 is involved in the regulation of the channels responsible for generating I_{K1}.

4.2. Depolarizing Na^+ and Ca^{2+} currents are altered in Cav-3KO myocytes

In addition to a decrease in repolarizing K^+ currents, increases in depolarizing Na^+ or Ca^{2+} currents can also prolong myocardial repolarization. Here, we demonstrate that there is an increase in $I_{Na,L}$ in Cav-3KO ventricular myocytes that contributes to APD prolongation, but peak I_{Na} is unchanged. Knockout of Cav-3 in iPSC-CMs in a recent study also showed

an increase in $I_{Na,L}$ without a change in peak I_{Na} [6]. Increased $I_{Na,L}$, due to acquired heart failure or inherited LQT3, is known to prolong APD and increase arrhythmia risk [49–51]. Prior studies have shown that co-expression of $Na_v1.5$ with WT Cav-3 does not alter either peak I_{Na} or $I_{Na,L}$ in HEK293 cells [14]. On the other hand, of the expression of the long QT associated Cav-3-F97C variant increases $I_{Na,L}$ in HEK293 cells, as well as APD in isolated mouse ventricular cardiomyocytes, via a mechanism that involves relief of Cav-3-dependent inhibitory S-nitrosylation of $Na_v1.5$ [52]. Our results are consistent with a loss of inhibitory S-nitrosylation of $Na_v1.5$ in the Cav-3KO myocytes, but future studies will be needed to specifically investigate the molecular mechanisms of this regulation given conflicting evidence regarding the subcellular localization of $Na_v1.5$ channel in caveolae or adjacent membrane domains [6, 53].

Our results also show a 28% reduction in peak $I_{Ca,L}$, as well as delayed inactivation of the current, in Cav-3KO myocytes. These changes in $I_{Ca,L}$ will have opposing effects on repolarization, and the net effect will be dependent on heart rate and the dynamic contributions from other ionic currents. In a recent report, we demonstrated Cav-3 variant-specific gain-of-function effects on $I_{Ca,L}$ for long QT associated variants when co-expressed with the channel in HEK293 cells [36]. While co-expression of Cav3-S141R increased $I_{Ca,L}$ density without changing the gating properties of the channel, Cav3-F97C reduced Ca^{2+}-dependent inactivation of $I_{Ca,L}$ without changing current density. Analysis of the relative contributions of ionic current alterations using computational modeling of the human ventricular myocyte action potential showed that the primary change responsible for prolonged APD was slowly inactivating $I_{Ca,L}$ in cells co-expressing Cav-3-F97C, whereas increased $I_{Ca,L}$ and $I_{Na,L}$ contributed equally to action potential prolongation in Cav-3-S141R-expressing cells. Thus, Cav-3 regulation of $I_{Ca,L}$ can impact repolarization and arrhythmia risk.

4.3. Caveolae regulation of ion channels and arrhythmia risk

Our data show that *Cav3* knockout in adult cardiomyocytes prolongs APD as a consequence of changes in multiple ionic currents. Interestingly, we did not find differences in the overall protein expression levels of $K_v4.2$, $K_v4.3$, $K_v1.4$, $K_v2.1$, KChIP2, $K_{ir}2.1$, $Ca_v1.2$, or $Na_v1.5$ between Cav-3KO and Con mouse myocardium, which suggests that the observed differences in ionic currents in myocytes from these mice are a consequence of altered channel gating or possible alterations in trafficking/recycling of channels to the sarcolemma. The precise molecular mechanism(s) underlying Cav-3-mediated regulation of individual ion channel proteins is poorly understood. Although multiple prior studies have suggested ion channels responsible for the altered ionic currents in the Cav-3KO mice are localized to caveolae as described above, a recent study using proximity-based as well as affinity-based mass spectrometry proteomics failed to identify any of these ion channel proteins as associated with Cav-3 [6]. Although the more unbiased assessment of Cav-3 associated proteins using these mass spectrometry approaches is powerful, low abundance transmembrane proteins may be below the detection limit or not readily identified by mass spectrometry. Nevertheless, superresolution imaging of cardiomyocytes has argued against co-localization of Nav1.5 with Cav-3 as observed with standard resolution confocal microscopy [6]. Instead, the labeling appears to be in proximal nanodomains but not

directly colocalized. For most of the other channel proteins investigated in this study, superresolution imaging or electron microscopic localization is not available, with the exception of $Ca_v1.2$ channels for which high resolution transmission electron microscopy showed co-immunogold labeling of $Ca_v1.2$ and Cav-3 in structural caveolae in neonatal and adult mouse cardiomyocytes [20, 54]. Thus for at least a subset of the channels a direct interaction with Cav-3 or associated scaffolding proteins could impact channel function as could the unique caveolar lipid composition.

Caveolae can also regulate ion channels by modulating signaling pathways and post-translational modifications that can impact channel function. Cav-3 has been reported to associate with a number of signaling proteins including nNOS, PKC, PI3K, and components of the β_2-adrenergic receptor signaling axis [7, 18, 20, 55]. Interestingly, evidence indicates that the PI3K signaling pathway plays an important role in the regulation of cardiac repolarization [56]. This is underscored by the fact that increased $I_{Na,L}$ as a result of defective PI3K signaling has been shown to underlie diabetes-induced QT prolongation [57]. Moreover, certain tyrosine kinase inhibitors used clinically as anti-cancer agents, such as nilotinib, also cause QT interval prolongation via a mechanism involving PI3K inhibition [58]. Therefore, loss of Cav-3 could prolong APD by inhibiting PI3K-mediated regulation of some ion channels. An additional signaling pathway linked to APD prolongation and Cav-3 results from disruption of nNOS-mediated ion channel regulation. We have previously shown that the long QTc-associated Cav-3-F97C variant increases $I_{Na,L}$ by preventing nNOS-dependent S-nitrosylation of $Na_v1.5$ [52]. Thus, disruption of nNOS-mediated S-nitrosylation of $Na_v1.5$ may underlie increased $I_{Na,L}$ in Cav-3KO myocytes. In a recent study, knockout of Cav-3 in human iPSCs prolonged APD as we observed, and those authors also demonstrated an increased in $I_{Na,L}$ [6]. Elucidation of the regulatory mechanism(s) underlying alterations in ionic currents in Cav-3KO myocytes will be the subject of important future work. Regardless, the findings of impaired repolarization in Cav-3KO hearts suggest that reduced Cav-3 levels and caveolae abundance can potentially lead to triggered arrhythmias (early afterdepolarizations) with dispersion of repolarization favoring reentry as observed in other forms of prolonged repolarization/QTc that increase the risk of ventricular arrhythmias. For example, reduced Cav-3 levels in certain forms of heart failure may be intimately involved in the risk of arrhythmia. Conversely, increased Cav-3 expression and caveolae promote cardioprotection from ischemia and blunt hypertrophic remodeling [28, 59–62], which suggests a potential protective effect from arrhythmias.

4.4. Study limitations

Although total protein levels of relevant ion channels did not differ in Cav-3KO and Con mouse ventricular myocardium, the possibility that altered cell surface expression of any of the impacted channels contributes to the observed differences in ionic currents cannot be ruled out without further experiments. Additionally, the sample size and variability in immunoblot protein expression studies cannot exclude small, but meaningful, changes in protein levels for the channels and regulatory proteins examined. The mechanism of ventricular arrhythmias at the cardiac tissue level observed in the Cav-3KO mice has not been experimentally defined and requires further investigation. Human iPSC-CMs exhibit an immature phenotype relative to adult native heart cardiomyocytes, which could impact their

response to alterations in Cav-3 levels. Future studies are necessary to determine the impact of Cav-3 knockdown on human iPSC-CM ionic currents and morphological caveolae.

5. Conclusions

In summary, we have generated cardiomyocyte-specific conditional Cav-3KO mice and show that the Cav-3KO mice have impaired ventricular repolarization reflected by a prolonged QT_c interval and an associated increased susceptibility to VT. Furthermore, in contrast to previous constitutive *Cav3* knockout models, these cardiac-specific Cav-3KO mice do not develop cardiac hypertrophy or heart failure. Using ventricular myocytes isolated from the hearts of Cav-3KO mice and mathematical modeling, we demonstrate that loss of Cav-3 and caveolae prolongs the mouse ventricular APD. In hiPSC-CMs, Cav-3 knockdown, likewise leads to APD prolongation, indicating that Cav-3 and caveolae are also important for the regulation of cardiac repolarization in human myocytes. These findings provide insight into the mechanism(s) of disrupted repolarization in some pathological cardiac conditions, such as heart failure and inherited or acquired arrhythmia syndromes.

Supplementary Material

Refer to Web version on PubMed Central for supplementary material.

Acknowledgements

The authors acknowledge the service of the University of Wisconsin Transgenic Animal Facility core in the generation of the transgenic mouse models used in this study. This work was funded by National Institutes of Heath grants R01 HL078878 (TJK, RCB), R01HL141214 (AG, TJK), R01 HL128598 (LLE), R01 HL139738–01 (LLE), S10RR025644 (TJK); British Heart Foundation RG/17/13/33173 (JG,CM); AHA 20POST35210239 (ZG).

Nonstandard abbreviation and Acronyms:

APD	Action potential duration
Cav-3	Caveolin-3
Cav-3KO	Cardiac-specific, conditional Caveolin-3 knockout mice
Cav-3Het	Cardiac-specific, conditional Caveolin-3 heterozygous knockout mice
MDP	Maximum diastolic potential
RMP	Resting membrane potential

References

[1]. Simons K, Toomre D, Lipid rafts and signal transduction, Nat Rev Mol Cell Biol 1(1) (2000) 31–9. [PubMed: 11413487]

[2]. Parton RG, McMahon KA, Wu Y, Caveolae: Formation, dynamics, and function, Curr Opin Cell Biol 65 (2020) 8–16. [PubMed: 32146331]

[3]. Razani B, Woodman SE, Lisanti MP, Caveolae: from cell biology to animal physiology, Pharmacol Rev 54(3) (2002) 431–67. [PubMed: 12223531]

[4]. Tang Z, Scherer PE, Okamoto T, Song K, Chu C, Kohtz DS, et al. , Molecular cloning of caveolin-3, a novel member of the caveolin gene family expressed predominantly in muscle, J Biol Chem 271(4) (1996) 2255–61. [PubMed: 8567687]

[5]. Galbiati F, Engelman JA, Volonte D, Zhang XL, Minetti C, Li M, et al. , Caveolin-3 null mice show a loss of caveolae, changes in the microdomain distribution of the dystrophin-glycoprotein complex, and t-tubule abnormalities, J Biol Chem 276(24) (2001) 21425–33. [PubMed: 11259414]

[6]. Peper J, Kownatzki-Danger D, Weninger G, Seibertz F, Pronto JRD, Sutanto H, et al. , Caveolin3 Stabilizes McT1-Mediated Lactate/Proton Transport in Cardiomyocytes, Circ Res 128(6) (2021) e102–e120. [PubMed: 33486968]

[7]. Patel HH, Murray F, Insel PA, Caveolae as organizers of pharmacologically relevant signal transduction molecules, Annu Rev Pharmacol Toxicol 48 (2008) 359–91. [PubMed: 17914930]

[8]. Maguy A, Hebert TE, Nattel S, Involvement of lipid rafts and caveolae in cardiac ion channel function, Cardiovasc Res 69(4) (2006) 798–807. [PubMed: 16405931]

[9]. Markandeya YS, Fahey JM, Pluteanu F, Cribbs LL, Balijepalli RC, Caveolin-3 regulates protein kinase A modulation of the Ca(V)3.2 (alpha1H) T-type Ca2+ channels, The Journal of biological chemistry 286(4) (2011) 2433–44. [PubMed: 21084288]

[10]. Pogwizd SM, Nonreentrant mechanisms underlying spontaneous ventricular arrhythmias in a model of nonischemic heart failure in rabbits, Circulation 92(4) (1995) 1034–48. [PubMed: 7543829]

[11]. Hegyi B, Bossuyt J, Ginsburg KS, Mendoza LM, Talken L, Ferrier WT, et al. , Altered Repolarization Reserve in Failing Rabbit Ventricular Myocytes: Calcium and beta-Adrenergic Effects on Delayed- and Inward-Rectifier Potassium Currents, Circulation. Arrhythmia and electrophysiology 11(2) (2018) e005852.

[12]. Barbagallo F, Xu B, Reddy GR, West T, Wang Q, Fu Q, et al. , Genetically Encoded Biosensors Reveal PKA Hyperphosphorylation on the Myofilaments in Rabbit Heart Failure, Circ Res 119(8) (2016) 931–43. [PubMed: 27576469]

[13]. Kim SY, Kim KH, Schilling JM, Leem J, Dhanani M, Head BP, et al. , Protective role of cardiac-specific overexpression of caveolin-3 in cirrhotic cardiomyopathy, Am J Physiol Gastrointest Liver Physiol 318(3) (2020) G531–G541. [PubMed: 31961720]

[14]. Vatta M, Ackerman MJ, Ye B, Makielski JC, Ughanze EE, Taylor EW, et al. , Mutant caveolin-3 induces persistent late sodium current and is associated with long-QT syndrome, Circulation 114(20) (2006) 2104–12. [PubMed: 17060380]

[15]. Vaidyanathan R, Markandeya YS, Kamp TJ, Makielski JC, January CT, Eckhardt LL, IK1-enhanced human-induced pluripotent stem cell-derived cardiomyocytes: an improved cardiomyocyte model to investigate inherited arrhythmia syndromes, Am J Physiol Heart Circ Physiol 310(11) (2016) H1611–21. [PubMed: 27059077]

[16]. Tyan L, Foell JD, Vincent KP, Woon MT, Mesquitta WT, Lang D, et al. , Long QT syndrome caveolin-3 mutations differentially modulate Kv 4 and Cav 1.2 channels to contribute to action potential prolongation, J Physiol 597(6) (2019) 1531–1551. [PubMed: 30588629]

[17]. Hagiwara Y, Sasaoka T, Araishi K, Imamura M, Yorifuji H, Nonaka I, et al. , Caveolin-3 deficiency causes muscle degeneration in mice, Human molecular genetics 9(20) (2000) 3047–54. [PubMed: 11115849]

[18]. Wright PT, Bhogal NK, Diakonov I, Pannell LMK, Perera RK, Bork NI, et al. , Cardiomyocyte Membrane Structure and cAMP Compartmentation Produce Anatomical Variation in β, Cell Rep 23(2) (2018) 459–469. [PubMed: 29642004]

[19]. Sohal DS, Nghiem M, Crackower MA, Witt SA, Kimball TR, Tymitz KM, et al. , Temporally regulated and tissue-specific gene manipulations in the adult and embryonic heart using a tamoxifen-inducible Cre protein, Circ Res 89(1) (2001) 20–5. [PubMed: 11440973]

[20]. Balijepalli RC, Foell JD, Hall DD, Hell JW, Kamp TJ, Localization of cardiac L-type Ca(2+) channels to a caveolar macromolecular signaling complex is required for beta(2)-adrenergic regulation, Proc Natl Acad Sci U S A 103(19) (2006) 7500–5. [PubMed: 16648270]

[21]. Harris SP, Bartley CR, Hacker TA, McDonald KS, Douglas PS, Greaser ML, et al. , Hypertrophic cardiomyopathy in cardiac myosin binding protein-C knockout mice, Circulation research 90(5) (2002) 594–601. [PubMed: 11909824]

[22]. Mitchell GF, Jeron A, Koren G, Measurement of heart rate and Q-T interval in the conscious mouse, The American journal of physiology 274(3 Pt 2) (1998) H747–51. [PubMed: 9530184]

[23]. Aschar-Sobbi R, Izaddoustdar F, Korogyi AS, Wang Q, Farman GP, Yang F, et al. , Increased atrial arrhythmia susceptibility induced by intense endurance exercise in mice requires TNFalpha, Nature communications 6 (2015) 6018.

[24]. Mawad D, Mansfield C, Lauto A, Perbellini F, Nelson GW, Tonkin J, et al. , A conducting polymer with enhanced electronic stability applied in cardiac models, Sci Adv 2(11) (2016) e1601007.

[25]. Laughner JI, Ng FS, Sulkin MS, Arthur RM, Efimov IR, Processing and analysis of cardiac optical mapping data obtained with potentiometric dyes, Am J Physiol Heart Circ Physiol 303(7) (2012) H753–65. [PubMed: 22821993]

[26]. Morotti S, Edwards AG, McCulloch AD, Bers DM, Grandi E, A novel computational model of mouse myocyte electrophysiology to assess the synergy between Na+ loading and CaMKII, J Physiol 592(6) (2014) 1181–97. [PubMed: 24421356]

[27]. Woodman SE, Park DS, Cohen AW, Cheung MW, Chandra M, Shirani J, et al. , Caveolin-3 knock-out mice develop a progressive cardiomyopathy and show hyperactivation of the p42/44 MAPK cascade, J Biol Chem 277(41) (2002) 38988–97. [PubMed: 12138167]

[28]. Markandeya YS, Phelan LJ, Woon MT, Keefe AM, Reynolds CR, August BK, et al. , Caveolin-3 Overexpression Attenuates Cardiac Hypertrophy via Inhibition of T-type Ca2+ Current Modulated by Protein Kinase Calpha in Cardiomyocytes, The Journal of biological chemistry 290(36) (2015) 22085–100. [PubMed: 26170457]

[29]. Feiner EC, Chung P, Jasmin JF, Zhang J, Whitaker-Menezes D, Myers V, et al. , Left ventricular dysfunction in murine models of heart failure and in failing human heart is associated with a selective decrease in the expression of caveolin-3, J Card Fail 17(3) (2011) 253–63. [PubMed: 21362533]

[30]. Cronk LB, Ye B, Kaku T, Tester DJ, Vatta M, Makielski JC, et al. , Novel mechanism for sudden infant death syndrome: persistent late sodium current secondary to mutations in caveolin-3, Heart Rhythm 4(2) (2007) 161–6. [PubMed: 17275750]

[31]. Gal DB, Wojciak J, Perera J, Tanel RE, Patel AR, Atrial standstill in a pediatric patient with associated caveolin-3 mutation, HeartRhythm Case Rep 3(11) (2017) 513–516. [PubMed: 29387541]

[32]. Xu H, Guo W, Nerbonne JM, Four kinetically distinct depolarization-activated K+ currents in adult mouse ventricular myocytes, The Journal of general physiology 113(5) (1999) 661–78. [PubMed: 10228181]

[33]. Anumonwo JM, Lopatin AN, Cardiac strong inward rectifier potassium channels, Journal of molecular and cellular cardiology 48(1) (2010) 45–54. [PubMed: 19703462]

[34]. Miake J, Marban E, Nuss HB, Biological pacemaker created by gene transfer, Nature 419(6903) (2002) 132–3.

[35]. Reilly L, Eckhardt LL, Cardiac potassium inward rectifier Kir2: Review of structure, regulation, pharmacology, and arrhythmogenesis, Heart Rhythm 18(8) (2021) 1423–1434. [PubMed: 33857643]

[36]. Tyan L, Foell JD, Vincent KP, Woon MT, Mesquitta WT, Lang D, et al. , Long QT syndrome caveolin-3 mutations differentially modulate K, J Physiol (2018).

[37]. Ma J, Guo L, Fiene SJ, Anson BD, Thomson JA, Kamp TJ, et al. , High purity human-induced pluripotent stem cell-derived cardiomyocytes: electrophysiological properties of action potentials and ionic currents, Am J Physiol Heart Circ Physiol 301(5) (2011) H2006–17. [PubMed: 21890694]

[38]. Kaab S, Nuss B, Chiamvimonvat N, O'Rourke B, Pak PH, Kass DA, et al. , Ionic mechanism of action potential prolongation in ventricular myocytes from dogs with pacing-induced heart failure, Circ Res 78 (1996) 262–273. [PubMed: 8575070]

[39]. Nabauer M, Beuckelmann DJ, Erdmann E, Characteristics of transient outward current in human ventricular myocytes from patients with terminal heart failure, Circ Res 73(2) (1993) 386–94. [PubMed: 8330381]

[40]. Nerbonne JM, Studying cardiac arrhythmias in the mouse--a reasonable model for probing mechanisms?, Trends Cardiovasc Med 14(3) (2004) 83–93. [PubMed: 15121155]

[41]. Alday A, Urrutia J, Gallego M, Casis O, α1-adrenoceptors regulate only the caveolae-located subpopulation of cardiac K(V)4 channels, Channels (Austin) 4(3) (2010) 168–78. [PubMed: 20224290]

[42]. Martens JR, Sakamoto N, Sullivan SA, Grobaski TD, Tamkun MM, Isoform-specific localization of voltage-gated K+ channels to distinct lipid raft populations. Targeting of Kv1.5 to caveolae, J Biol Chem 276(11) (2001) 8409–14. [PubMed: 11115511]

[43]. Folco EJ, Liu GX, Koren G, Caveolin-3 and SAP97 form a scaffolding protein complex that regulates the voltage-gated potassium channel Kv1.5, Am J Physiol Heart Circ Physiol 287(2) (2004) H681–90. [PubMed: 15277200]

[44]. Eldstrom J, Van Wagoner DR, Moore ED, Fedida D, Localization of Kv1.5 channels in rat and canine myocyte sarcolemma, FEBS Lett 580(26) (2006) 6039–46. [PubMed: 17054951]

[45]. Martens JR, Navarro-Polanco R, Coppock EA, Nishiyama A, Parshley L, Grobaski TD, et al. , Differential targeting of Shaker-like potassium channels to lipid rafts, J Biol Chem 275(11) (2000) 7443–7446. [PubMed: 10713042]

[46]. Tristani-Firouzi M, Jensen JL, Donaldson MR, Sansone V, Meola G, Hahn A, et al. , Functional and clinical characterization of KCNJ2 mutations associated with LQT7 (Andersen syndrome), J Clin Invest 110(3) (2002) 381–8. [PubMed: 12163457]

[47]. Vaidyanathan R, Vega AL, Song C, Zhou Q, Tan BH, Tan B, et al. , The interaction of caveolin 3 protein with the potassium inward rectifier channel Kir2.1: physiology and pathology related to long qt syndrome 9 (LQT9), J Biol Chem 288(24) (2013) 17472–80. [PubMed: 23640888]

[48]. Vaidyanathan R, Van Ert H, Haq KT, Morotti S, Esch S, McCune EC, et al. , Inward Rectifier Potassium Channels (Kir2.x) and Caveolin-3 Domain-Specific Interaction: Implications for Purkinje Cell-Dependent Ventricular Arrhythmias, Circ Arrhythm Electrophysiol 11(1) (2018) e005800.

[49]. Maier LS, A novel mechanism for the treatment of angina, arrhythmias, and diastolic dysfunction: inhibition of late I(Na) using ranolazine, Journal of cardiovascular pharmacology 54(4) (2009) 279–86. [PubMed: 19333133]

[50]. Shryock JC, Song Y, Rajamani S, Antzelevitch C, Belardinelli L, The arrhythmogenic consequences of increasing late INa in the cardiomyocyte, Cardiovascular research 99(4) (2013) 600–11. [PubMed: 23752976]

[51]. Antzelevitch C, Nesterenko V, Shryock JC, Rajamani S, Song Y, Belardinelli L, The role of late I Na in development of cardiac arrhythmias, Handbook of experimental pharmacology 221 (2014) 137–68. [PubMed: 24737235]

[52]. Cheng J, Valdivia CR, Vaidyanathan R, Balijepalli RC, Ackerman MJ, Makielski JC, Caveolin-3 suppresses late sodium current by inhibiting nNOS-dependent S-nitrosylation of SCN5A, J Mol Cell Cardiol 61 (2013) 102–10. [PubMed: 23541953]

[53]. Cheng J, Valdivia CR, Vaidyanathan R, Balijepalli RC, Ackerman MJ, Makielski JC, Caveolin-3 suppresses late sodium current by inhibiting nNOS-dependent S-nitrosylation of SCN5A, J Mol Cell Cardiol 61 (2013) 102–10. [PubMed: 23541953]

[54]. Balijepalli RC, Kamp TJ, Caveolae, ion channels and cardiac arrhythmias, Prog Biophys Mol Biol 98(2–3) (2008) 149–60. [PubMed: 19351512]

[55]. Wright PT, Nikolaev VO, O'Hara T, Diakonov I, Bhargava A, Tokar S, et al. , Caveolin-3 regulates compartmentation of cardiomyocyte beta2-adrenergic receptor-mediated cAMP signaling, Journal of molecular and cellular cardiology 67 (2014) 38–48. [PubMed: 24345421]

[56]. Ballou LM, Lin RZ, Cohen IS, Control of cardiac repolarization by phosphoinositide 3-kinase signaling to ion channels, Circulation research 116(1) (2015) 127–37. [PubMed: 25552692]

[57]. Lu Z, Jiang YP, Wu CY, Ballou LM, Liu S, Carpenter ES, et al. , Increased persistent sodium current due to decreased PI3K signaling contributes to QT prolongation in the diabetic heart, Diabetes 62(12) (2013) 4257–65. [PubMed: 23974924]

[58]. Lu Z, Wu CY, Jiang YP, Ballou LM, Clausen C, Cohen IS, et al. , Suppression of phosphoinositide 3-kinase signaling and alteration of multiple ion currents in drug-induced long QT syndrome, Science translational medicine 4(131) (2012) 131ra50.

[59]. Fridolfsson HN, Patel HH, Caveolin and caveolae in age associated cardiovascular disease, J Geriatr Cardiol 10(1) (2013) 66–74. [PubMed: 23610576]

[60]. Tsutsumi YM, Horikawa YT, Jennings MM, Kidd MW, Niesman IR, Yokoyama U, et al. , Cardiac-specific overexpression of caveolin-3 induces endogenous cardiac protection by mimicking ischemic preconditioning, Circulation 118(19) (2008) 1979–88. [PubMed: 18936328]

[61]. Sinha B, Köster D, Ruez R, Gonnord P, Bastiani M, Abankwa D, et al. , Cells respond to mechanical stress by rapid disassembly of caveolae, Cell 144(3) (2011) 402–13. [PubMed: 21295700]

[62]. Horikawa YT, Panneerselvam M, Kawaraguchi Y, Tsutsumi YM, Ali SS, Balijepalli RC, et al. , Cardiac-specific overexpression of caveolin-3 attenuates cardiac hypertrophy and increases natriuretic peptide expression and signaling, J Am Coll Cardiol 57(22) (2011) 2273–83. [PubMed: 21616289]

Highlights

- *Cav3* knockout in adult mouse heart does not impact basal contractile function.
- Cardiac-specific knockout of *Cav3* greatly reduces caveolae in cardiomyocytes.
- Loss of Cav-3 delays repolarization in mice by affecting multiple ionic currents.
- *Cav3* knockout in mouse heart increases susceptibility to ventricular arrhythmia.
- Knockdown of Cav-3 also delays repolarization in human iPSC-cardiomyocytes.

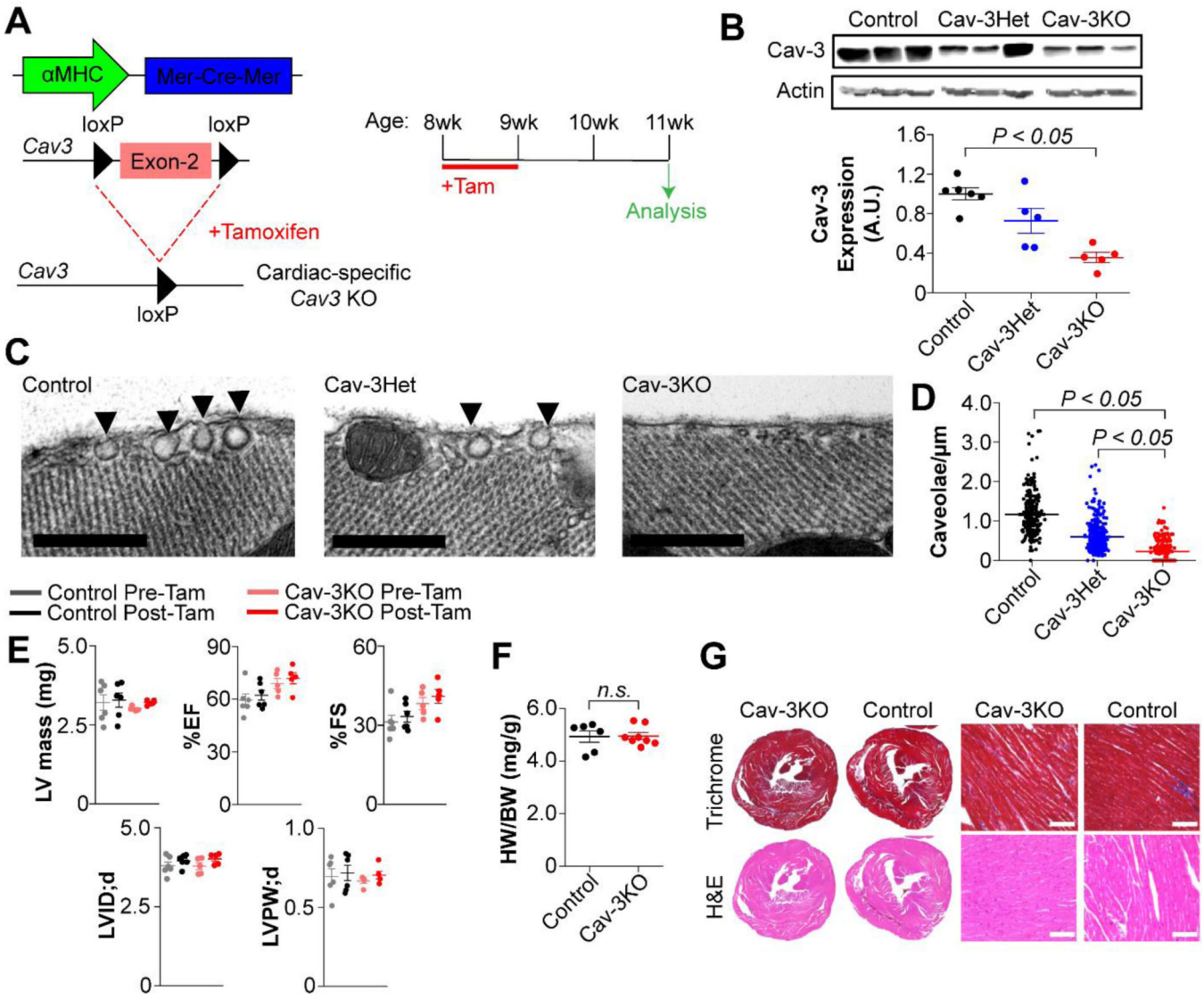

Fig. 1. Cardiac-specific Cav3 knockout mice exhibit reduced Cav-3 expression and decreased cardiomyocyte caveolae but have normal macroscopic cardiac structure and contractile function.

(A) Schematic representation of Tamoxifen (Tam)-inducible activation of αMHC-MerCreMer for cardiac-specific Cav-3 knockout mouse generation and timeline for experiments. (B) Immunoblot and quantification of relative Cav-3 expression to loading control actin from left ventricle of Control (n = 6), Cav-3Het (n = 5), and Cav-3KO (n = 5) mice (one-way ANOVA with post hoc Tukey method). (C) Transmission electron micrographs of left ventricle sections (scale bar 500 nm). Morphological caveolae are denoted by arrow heads. (D) Caveolae per micron membrane from Control (n = 242 images), Cav-3Het (n = 342 images), and Cav-3KO (n = 437 images) mice from 3 animals per group. (E) Assessment of cardiac function by echocardiographic parameters before and after Tam treatment in Control and Cav-3KO mice (3–5 animals per group, n.s. by 2-tailed paired t-test before and after Tam). (F) Heart weight/body weight (HW/BW) ratios (Control n = 6, Cav-3KO n = 8, n.s. by 2-tailed unpaired t-test). (G) Histological assessment of

mid-LV transverse section Control and Cav-3KO hearts stained with Masson’s trichrome and H&E. Scale bars 100 μm.

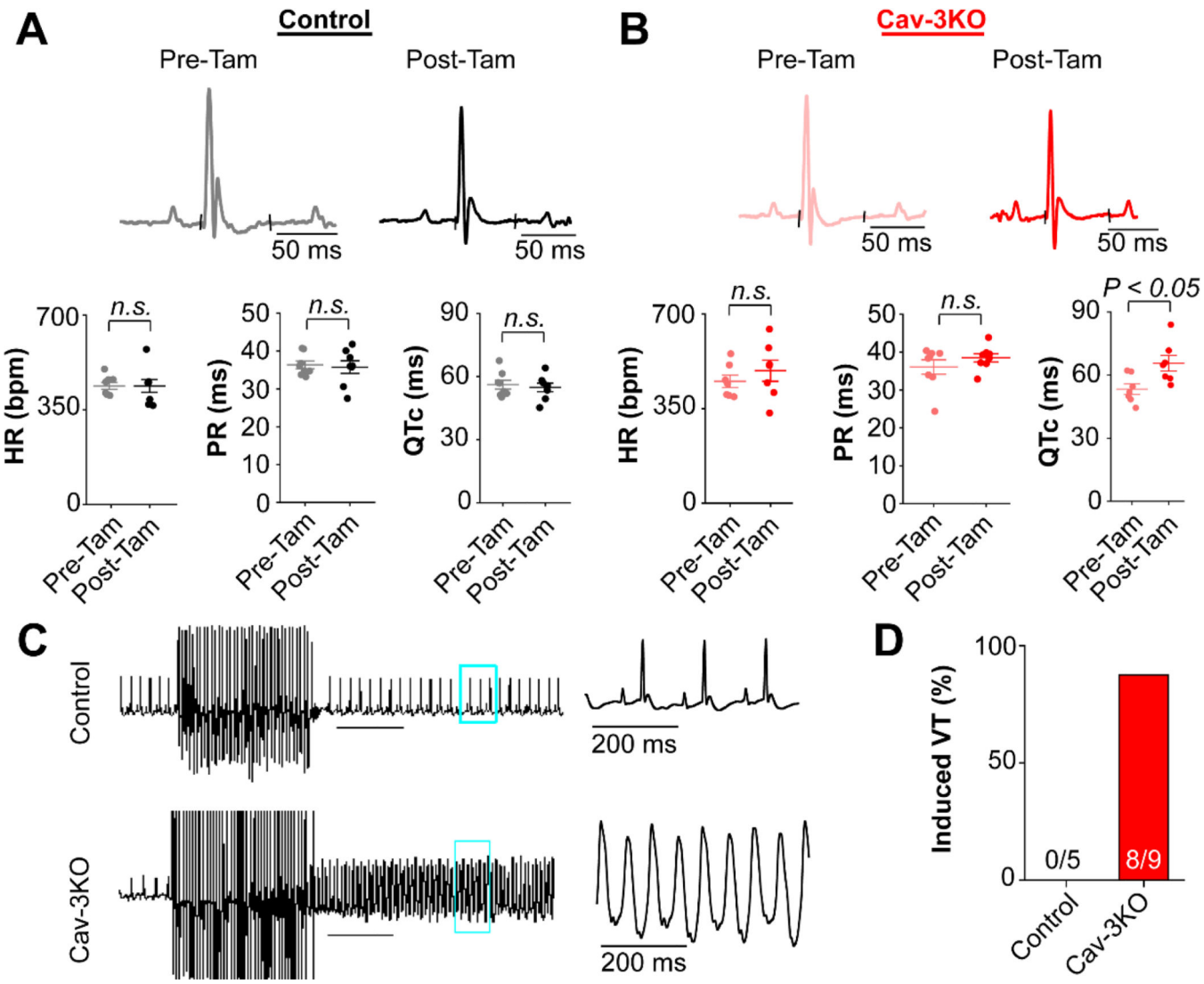

Fig. 2. Cav-3KO mice exhibit prolonged QTc interval and increased susceptibility to ventricular arrhythmia.

(A, B) Representative single ECG complex, measured heart rate, PR interval, and QTc interval before and after Tam treatment for Con and Cav-3KO mice (n = 7–8 for QTc measurement and n = 7–8 for HR, statistical comparisons by two-tailed paired t-tests), with Cav-3KO mice showing significant QTc prolongation post-Tam. (C) Representative traces of ventricular tachycardia (VT) induced with ventricular burst pacing from Con and Cav-3KO mice enlarged on right (scale bar 1 sec). (D) Comparison of induced VT incidence in mice ($P < 0.001$, chi-square statistic is 10.37). Tam treatment was for 1 week and after another 2 weeks animals were studied.

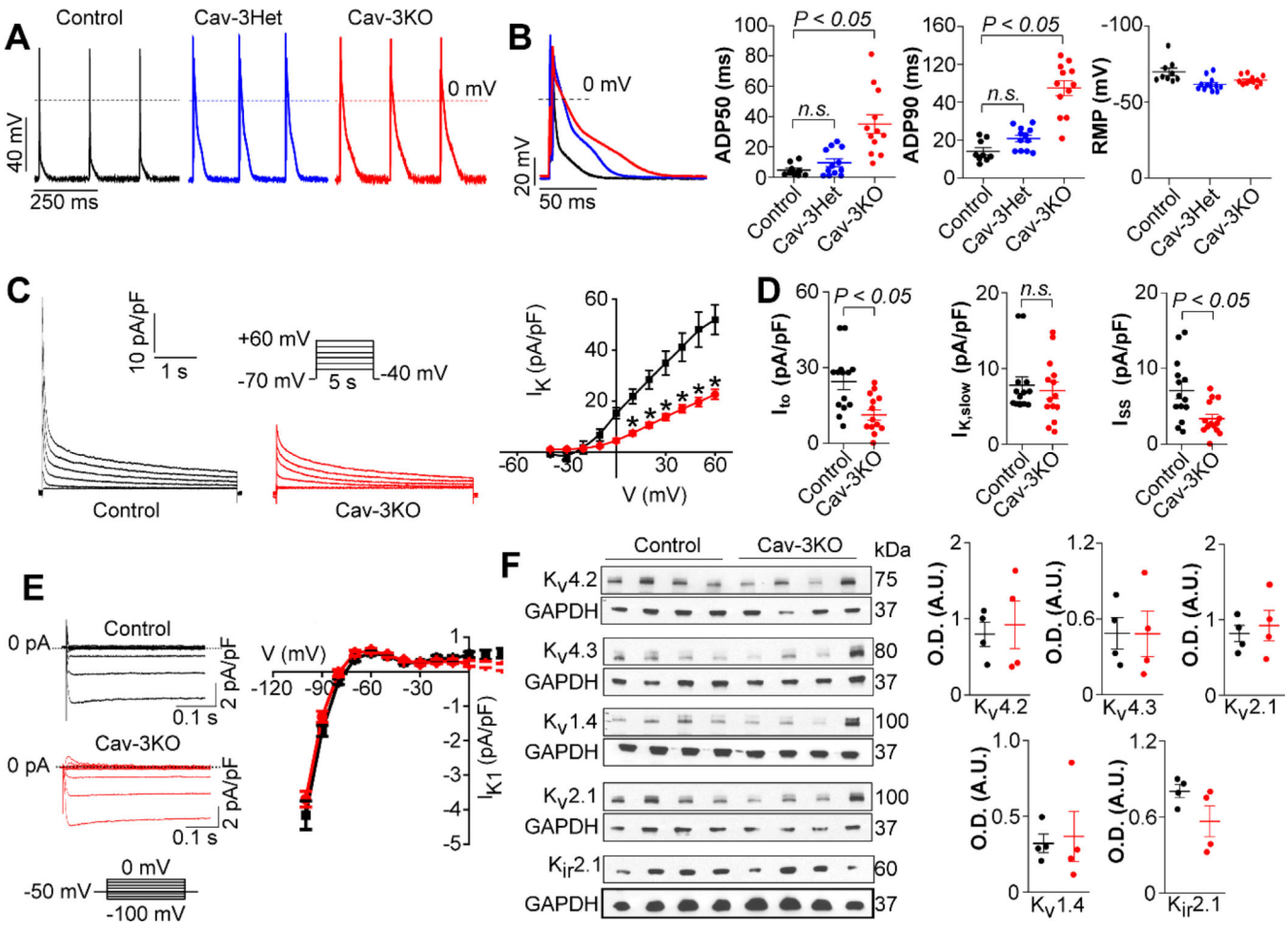

Fig. 3. Loss of Cav-3 expression in ventricular myocytes prolongs APD and reduces I_{to} and I_{ss} current densities.

(A) Representative traces of ventricular action potentials from Con, Cav-3Het and Cav-3KO mice simulated at a rates of 5 Hz at 37 ± 2 °C. (B) Comparison of action potential traces, mean APD50, mean APD90, and resting membrane potential (RMP) from Con (n = 9), Cav-3Het (n = 13), and Cav-3KO (n = 13) myocytes from 4–5 mice per group (one-way ANOVA with post hoc Tukey method) (C) Representative traces of I_K and I-V relationships with respect to different test potentials from Con (n = 14) and Cav-3KO (n = 14) myocytes from 4 animals per group (*P<0.05 by two tailed unpaired t-test). Voltage protocols is shown in panel inset. (D) Mean I_{to}, I_{Kslow}, and I_{ss} determined by bi-exponential curve fit for the decay phase of I_K at +40 mV test pulse (two tailed unpaired t-test for comparisons). (E) Representative traces of I_{K1} and I-V relationships for I_{K1} from Con (n = 16) and Cav-3KO (n = 9) myocytes from 3 animals per group. (F) Representative Western blots showing $K_v4.2$, $K_v4.3$, $K_v2.1$, $K_v1.4$, and $K_{ir}2.1$ protein levels from left ventricular lysates prepared from Con and Cav-3KO mice. Right panel, is summary data of relative K^+ channel expression normalized to GAPDH (n = 4).

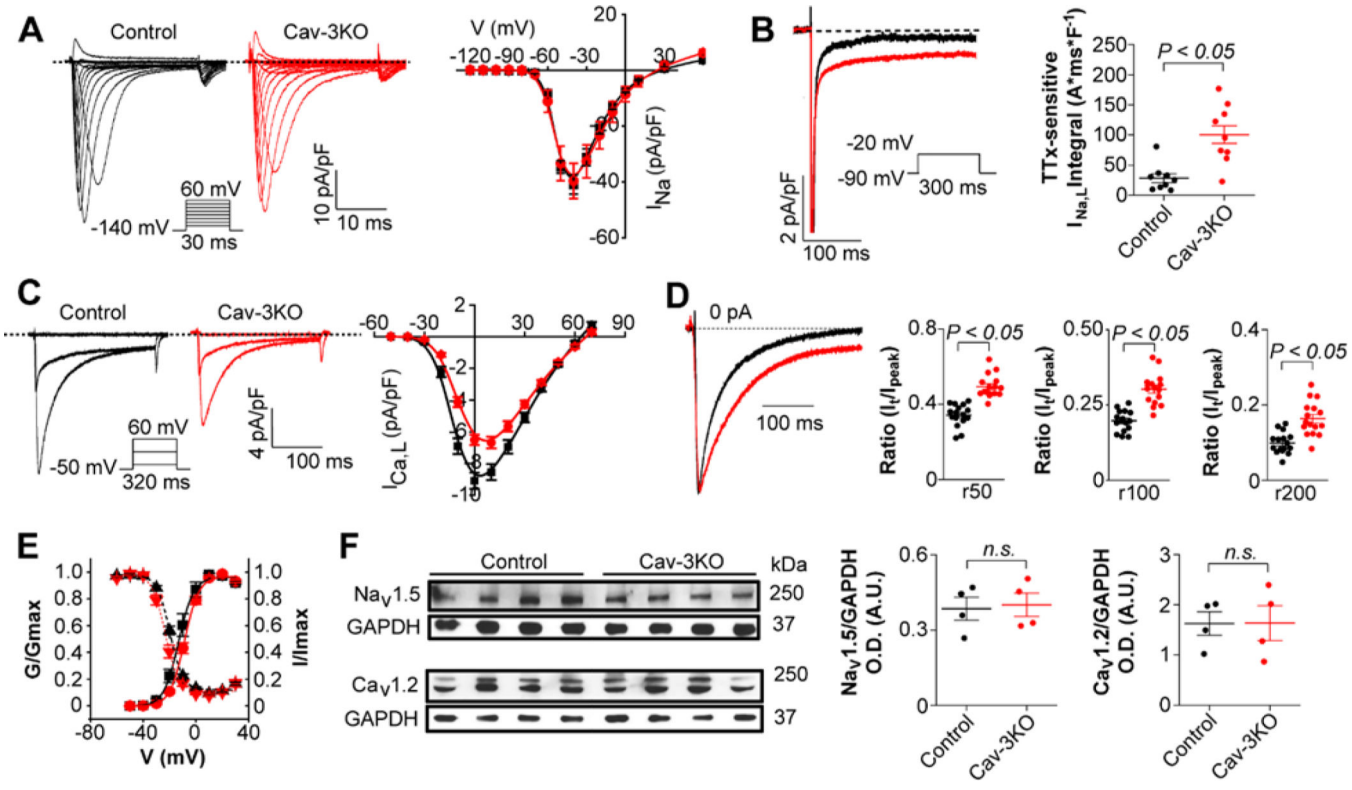

Fig. 4. Increased $I_{Na,L}$ and reduced $I_{Ca,L}$ with delayed inactivation in Cav-3KO ventricular myocytes.

(A) Representative traces of I_{Na} and I-V relationships from Con (n = 7, 3 mice) and Cav-3KO (n = 13, 5 mice) myocytes. (B) Representative traces of $I_{Na,L}$ from Con and Cav-3KO myocytes and average integrals of TTX-sensitive $I_{Na,L}$ measured between 50 and 300 ms from Con (n = 10, 3 mice) and Cav-3KO (n = 11, 3 mice) myocytes. (C) Representative traces of $I_{Ca,L}$ and I-V relationships from Con (n = 11, 4 mice) and Cav-3KO (n = 17, 4 mice) myocytes (*p < 0.001). (D) Representative traces of $I_{Ca,L}$ normalized to peak, indicating delayed $I_{Ca,L}$ inactivation. The mean residual current at 50, 100, and 200 ms from peak during 0 mV test pulse. (E) Steady state inactivation and activation plots for Con and Cav-3KO myocytes. Mean fit parameters to inactivation data for Con (n = 9) and Cav-3KO (n=16), respectively, are $V_{1/2}$ = −23.3 ± 1.1 mV and = −19.7 ± 0.67 mV (P ≤ 0.05), k = 4.5 ± 0.2 and 4.8 ± 0.2, (n.s.). Mean fit parameters for activation data for Con (n = 8) and Cav-3 (n=15), respectively, are $V_{1/2}$ = − 10.97 ± 0.6 mV and − 8.73± 0.51 mV (n.s.), k = 4.86 ± 0.2 and 5.13 ± 0.26, (n.s.). (F) Representative Western blot analysis of $Na_v1.5$, $Ca_v1.2$, and GAPDH expression in Con and Cav-3KO heart lysates. Right panel, relative $Na_v1.5$, $Ca_v1.2$ protein expression levels normalized to GAPDH (n = 4, repeated 3 times). Voltage protocols are as shown in figure insets. Statistical comparisons use two-tailed, unpaired t-test. n.s.=no significant difference.

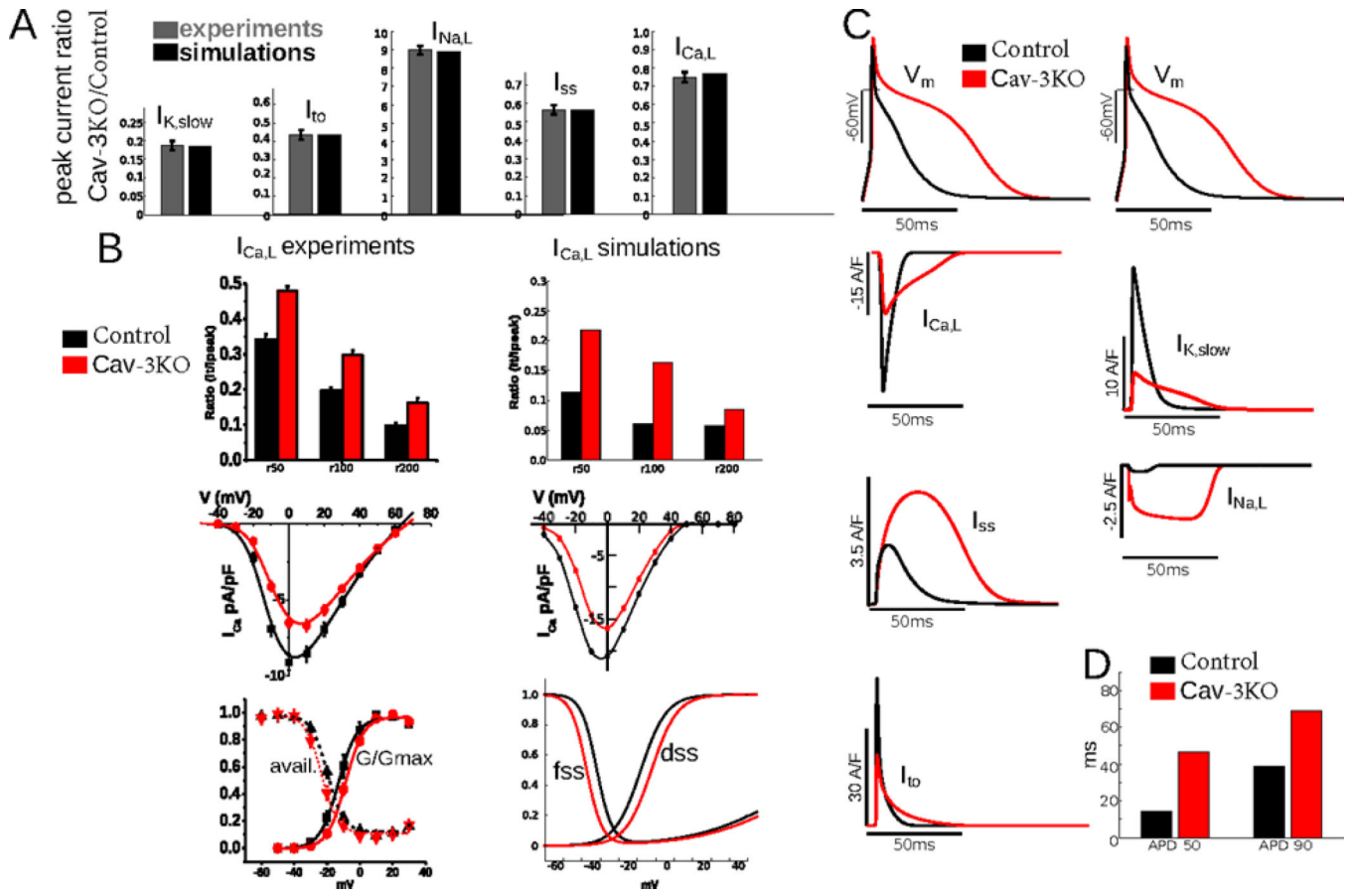

Fig. 5. Numerical simulations of action potentials from Morrotti et al. mouse ventricular cell model recapitulate the prolonged action potential duration with loss of Cav-3.

(A) Summary of Cav-3KO/Con peak current ratios for $I_{K,slow}$, I_{to}, $I_{Na,L}$, I_{ss}, and $I_{Ca,L}$ currents measured experimentally and employed for mathematical modeling. (B) Mathematical modeling accurately reproduced the time dependence of relative $I_{Ca,L}$ current observed experimentally in Cav-3KO. WT in black and Cav-3KO in red. Experiments left and simulations right. Top: time dependence of current ratio at 50, 100 and 200 ms. Middle: peak IV-curve, Bottom: steady state activation, dss, and inactivation, fss). (C) Top: simulated action potential traces with loss of Cav-3 showing longer APD. Bottom: Superimposed traces of simulated $I_{Ca,L}$, $I_{K,slow}$, I_{ss} $I_{Na,L}$, I_{to}, for Cav-3KO and Con myocytes. (D) Mean APD50 and mean APD90 from simulated Con and Cav-3KO myocyte action potentials. Free running action potential (AP) simulations showed dynamic changes in currents at 1 Hz steady state pacing, and a prolonging effect of Cav-3KO on the APD50 and APD90. Con in black and Cav-3KO traces in red.

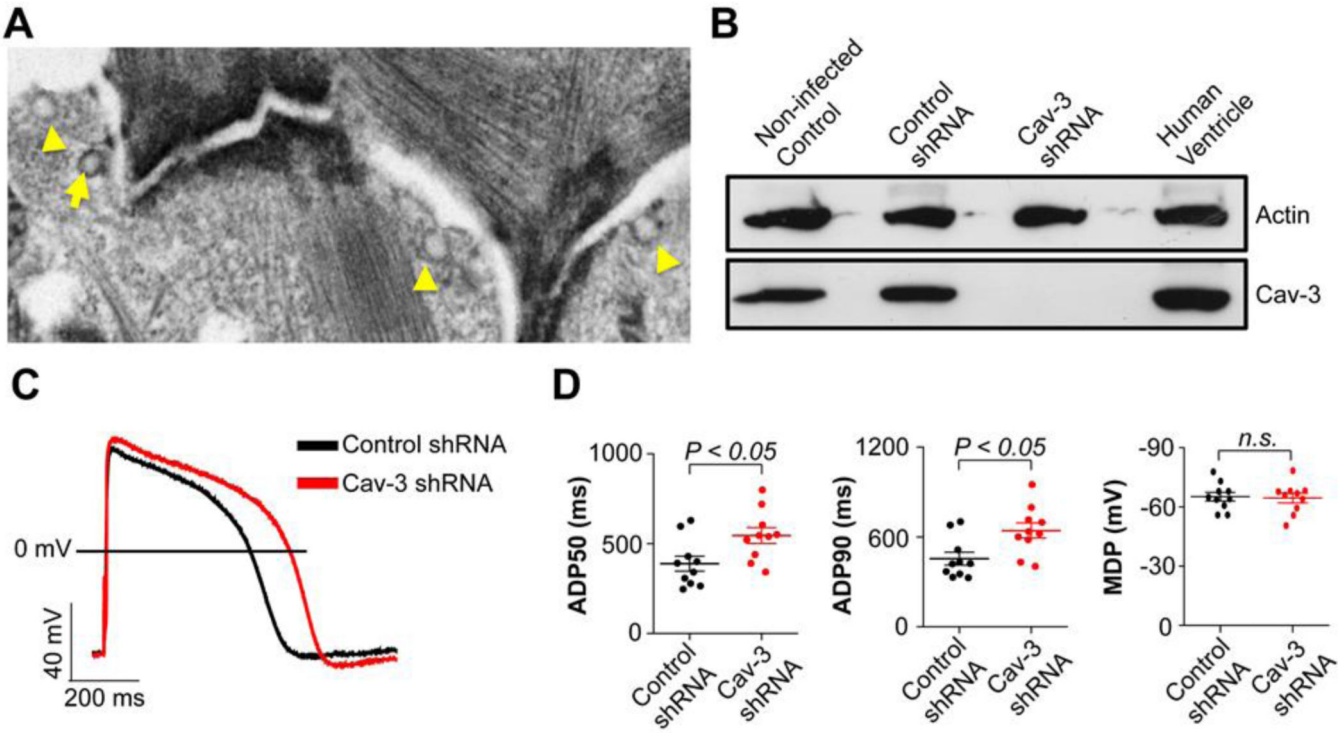

Fig. 6. shRNA-mediated Cav-3 knockdown in hiPSC-CMs prolongs APD.

(A) Representative transmission electron micrograph of hiPSC-CMs with morphological caveolae denoted with arrow heads (scale bar 500 μm). (B) Representative Western blot showing loss of Cav-3 protein in lentiviral Cav-3 shRNA infected hiPSC-CMs. (C) Representative traces of action potentials from scrambled shRNA and Cav-3 shRNA infected hiPSC-CMs. (D) Comparison of MDP, APD50, and APD90 from Con and Cav-3 shRNA infected hiPSC-CMs (n = 10 cells from 4 different infections).